J Mater Sci (2008) 43:102–116
DOI 10.1007/s10853-007-2124-6

Some aspects of workability studies on sintered high strength P/M steel composite preforms of varying TiC contents during hot forging

R. Narayanasamy · V. Senthilkumar · K. S. Pandey

Received: 20 October 2006 / Accepted: 21 August 2007 / Published online: 27 September 2007

Abstract Workability is a measure of the extent of deformation that powder metallurgy materials can withstand prior to fracture occurred in the forming or upsetting processes. Workability of a material is obtained from several parameters namely strain, strain rate and temperature. Hot upsetting of the composite steel preforms with varying TiC contents, namely, 3% and 4%, and aspect ratios, namely, 0.45, 0.71 and 1.25, was carried out at a temperature of 1120 °C and the formability behaviour of the same under triaxial stress state condition was determined. The curves plotted for different preforms were analysed and a relationship was established between the axial strain and the formability stress index (β). The influence of TiC addition, in the steel composite, on the formability stress index, the relative density (R) and various stress ratio parameters, namely, ($\sigma_\theta/\sigma_{eff}$), ($\sigma_m/\sigma_{eff}$) and ($\sigma_z/\sigma_{eff}$) were studied. An attempt is also made to relate the fracture strain of the preforms with the formability stress index (β) under triaxial stress state condition.

Nomenclature

h_o	Initial preform height
h_f	Deformed height of the preform
D_o	Initial diameter of the preform
D_{c1}	Contact diameter of the preform (top surface)
D_{c2}	Contact diameter of the preform (bottom surface)
D_c	Contact diameter
D_b	Bulged diameter
R	Relative density
ρ_o	Initial preform density
ρ_{th}	Theoretical preform density
ρ_f	Deformed preform density
σ_θ	True Hoop stress
σ_z	True axial stress
σ_r	True radial stress
σ_m	Mean or hydrostatic stress
σ_{eff}	Effective stress
ε_z	True axial strain
ε_θ.	True hoop strain
γ	Poisson's ratio
R_1	Barrel radius
R_2^2	Correlation coefficient

Introduction

Workability is a measure of the extent of deformation that powder metallurgy materials can withstand prior to fracture occurred in the forming or upsetting processes. Research carried out in workability of fully dense materials indicates that careful control of the deformation can reduce or eliminate the local stress and strain states that lead to fracture [1, 2]. The occurrence of ductile fracture during plastic deformation is a dangerous factor in many metal working processes. The prediction of fracture in the

R. Narayanasamy · V. Senthilkumar (✉)
Department of Production Engineering, National Institute of Technology, Tiruchirappalli, Tamil Nadu 620 015, India
e-mail: mrvsk@rediffmail.com

R. Narayanasamy
e-mail: narayan@nitt.edu

K. S. Pandey
Department of Metallurgical Engineering, National Institute of Technology, Tiruchirappalli, Tamil Nadu 620 015, India

design stage itself and its early modification can save a lot of money. Kuhn and Downey [3] investigated the deformation characteristics and plasticity theory of sintered powder materials and studied the basic deformation behaviour of sintered iron powder performing simple homogeneous compression tests and also proposed a plasticity theory relating yield stress and Poisson's ratio to the density. A plasticity theory for porous metals was presented by Shima and Oyane [4] and was applied to frictionless closed-die compression and the stress in the direction of compression has been evaluated in relation to the relative density. A new yield function for compressible powder metallurgy materials was suggested by Doraivelu et al. [5]. The yield function has been derived based upon a yield criterion and this function was experimentally verified for the uniaxial state of compressive stress using the P/M aluminium alloy but this function as not verified with other state of stresses. An excellent work was carried out by Abdel-Rahman and El-Sheik [6] on workability in the forging of powder metallurgy compacts. The effect of the relative density on the forming limit of P/M compacts in upsetting was investigated and a workability factor was presented for the case of uniaxial stress state condition which describes the effect of the mean and the effective stresses (σ_m and σ_{eff}).

Sowerby et al. [7] made an attempt in their research work on the effective use of hoop (ε_θ) and the axial strains (ε_z) at the free surface of an upsetting specimen and from which they obtained the associated stress. Rao and Hawbolt [8] developed a constitutive relationship using the compression testing of medium carbon steel. Flow curves for the hot deformation in compression was obtained using a computer controlled thermo-mechanical simulator and the flow stress was described in terms of process variables, strain, strain rate and temperature. A new generalized yield criterion was pointed out by Park [9] and two relations (among parameters namely, plastic Poisson's ratio, the relative density and flow stress of the matrix material) were obtained through experiments. In the above reference, several yield criteria for sintered powder material were also compared with each other. A new generalized yield criterion of porous sintered P/M metals was discussed by Narayanasamy and Ponalagusamy [10], considering an anisotrophic parameter. In addition, a new flow rule with anistrophic parameter for porous metal was also proposed. Microscopic voids in any ductile material play a vital role in various fractures. Tvergaard [11] analysed the macroscopic properties of a porous ductile medium on the basis of an axisymmetric numerical model. A new densification model for porous metallic powder material was proposed by Zhou et al. [12] for controlling the porosity of the powder materials and simulated the compression of a sintered cylinder using MSC (Marc Software Corporations). Gouveia et al. [13] predicted the initiation of the ductile fracture after conducting experiments on powder compacts with various geometrical shapes such as ring, cylindrical, tapered and flanged under several different loading conditions. Narayanasamy et al. [14] presented some of the important criteria generally used for the prediction of ductile fracture. The integrals of stress functions were used for the proposal of simple ductile criterion. A large deformation finite element simulation was studied by Venugopal Rao et al. [15] for comparing the evaluation of theoretical failure criteria for workability in cold forming and compared the experimental values of different aspect ratios with those obtained through FEA of complex metal working process at fracture, VIDHAN (an in-house developed elastoplastic large deformation FEM based software package) was used for the simulation. An advanced method is developed for optimal control of the then mechanical parameters during hot plastic working processes of advanced materials by Feng and Luo [16] based on the finite element method and modern optimal control theory. The ram velocity profile to obtain high quality forgings was developed and the proposed method also lays the theoretical foundation for the open-loop control of forging processes for difficult-to-deform materials.

In the present study, two different steel composites, namely, 3% and 4% TiC, with different aspect ratios, namely, 0.45, 0.71 and 1.25, are investigated in hot forging under triaxial stress condition to analyse the influence of percentage addition of TiC, in the steel composites, on various workability parameters such as the formability stress index (β) and the various stress ratios, namely, ($\sigma_\theta/\sigma_{eff}$), ($\sigma_m/\sigma_{eff}$) and ($\sigma_z/\sigma_{eff}$).

Theoretical analysis

The mathematical expressions used and proposed for the determination of various upsetting parameters of upsetting for various stress state conditions are discussed below.

Plane stress conditions

According to Abdel Rahman and El-Sheik [6], the expression for the axial or height strain (ε_z) can be written as follows:

$$\varepsilon_z = \ln[h_f/h_o] \quad (1)$$

where, h_o is the initial height and h_f is the deformed height of the preform.

According to Narayanasamy and Pandey [17], the expression for the new hoop strain (ε_θ) is as follows:

$$\varepsilon_\theta = \ln[(2D_b^2 + D_c^2)/(3D_0^2)] \quad (2)$$

where, D_b is the bulge diameter, D_o is the initial diameter and D_c is the average contact diameter of the preform. The average diameter of the preform is expressed as follows:

$$D_c = (D_{c1} + D_{c2})/2$$

In the above expression for the average contact diameter of the preform, D_{c1} is the contact diameter of the preform at top and D_{c2} is the contact diameter of the preform at bottom.

Further from the above reference [17], the state of stress in a plane stress condition and the associated flow characteristics for porous materials can be expressed as follows:

$$\frac{d\varepsilon_\theta}{d\varepsilon_z} = \left(\frac{\sigma_\theta - \gamma\sigma_z}{\sigma_z - \gamma\sigma_\theta}\right) \quad (3)$$

$d\varepsilon_z$ is the plastic strain increment in axial direction, $d\varepsilon_\theta$, the plastic strain increment in the hoop direction, σ_z, the true axial stress, σ_θ, the true hoop stress and γ is the Poisson's ratio expressed as below:

$$\gamma = \left(\frac{\varepsilon_\theta}{2\varepsilon_z}\right) \quad (4)$$

Equation 3 can be further simplified as follows:

$$\frac{\sigma_\theta}{\sigma_z} = \left(\frac{\alpha + \gamma}{1 + \alpha\gamma}\right) \quad (5)$$

where, $\alpha = d\varepsilon_\theta/d\varepsilon_z$.

According to Narayansamy and Pandey [18], the expression for the hydrostatic stress (σ_m) can be written as below:

$$\sigma_m = \frac{1}{3}(\sigma_\theta + \sigma_z) \quad (6)$$

Since σ_r is considered to be zero in the case of plane stress condition the Eq. 6 can be written as follows:

$$\frac{\sigma_m}{\sigma_z} = \frac{1}{3}\left(1 + \frac{\sigma_\theta}{\sigma_z}\right) \quad (7)$$

According to Narayanasamy and Pandey [19], the relationship between the effective stress (σ_{eff}) and the axial stress (σ_z) can be written as follows:

$$\sigma_{eff} = (0.5 + \alpha)\left[3(1 + \alpha + \alpha^2)\right]^{0.5}\sigma_z \quad (8)$$

where, σ_{eff} is the effective stress, α is the strain increment ratio ($d\varepsilon_\theta/d\varepsilon_z$) and σ_z is the axial stress.

The Eq. 8 can be rearranged as follows:

$$\frac{\sigma_{eff}}{\sigma_z} = (0.5 + \alpha)\left[3(1 + \alpha + \alpha^2)\right]^{0.5} \quad (9)$$

From the Eqs. 3 and 7, the expression for the stress ratio (σ_{eff}/σ_z) is as given below:

$$\frac{\sigma_{eff}}{\sigma_z} = \frac{1}{M}\left(\frac{\alpha + \gamma}{1 + \gamma\alpha}\right) \quad (10)$$

where,

$$M = (0.5 + \alpha)\left[3(1 + \alpha + \alpha^2)\right]^{0.5}$$

As an evidence of experimental investigation implying the importance of the spherical component of the stress state on fracture according to Vujovic and Shabaik [20] proposed a parameter called a formability stress index 'β' given by,

$$\beta = [3\sigma_m/\sigma_{eff}] \quad (11)$$

This index determines the fracture limit as explained in the Ref. [21].

The stress formability index (β) can be expressed from Eqs. 5 and 8 as follows:

$$\beta = 3\{[\sigma_m/\sigma_z]/[1/[\sigma_{eff}/\sigma_z]]\} \quad (12)$$

Triaxial stress state condition

According to Narayansamy and Pandey [18], for the state of stress under triaxial stress state condition is given as below:

$$\alpha = \frac{A}{B} \quad \alpha = \frac{d\varepsilon_\theta}{d\varepsilon_z} \quad (13)$$

where

$$A = \left[(2 + R^2)\sigma_\theta - R^2(\sigma_z + 2\sigma_\theta)\right]$$
$$B = \left[(2 + R^2)\sigma_z - R^2(\sigma_z + 2\sigma_\theta)\right]$$

where, α is the strain increment ratio and R is the relative density. From the above Eq. 13, for the known values of α, R and the axial stress, σ_z, the hoop stress component, σ_θ, can be determined as given below:

$$\sigma_\theta = \left[\frac{2\alpha + R^2}{2 - R^2 + 2R^2\alpha}\right]\sigma_z \quad (14)$$

Rearranging the above Eq. 14, the expression for the stress ratio (σ_θ/σ_z) can be expressed as given below:

$$\frac{\sigma_\theta}{\sigma_z} = \left[\frac{2\alpha + R^2}{2 - R^2 + 2R^2\alpha}\right] \tag{15}$$

In the above Eq. 15, relative density (R) plays a major role in finding the hoop stress component (σ_θ).

It is assumed that $\sigma_r = \sigma_\theta$ for the case of axisymmetric condition. It is known that the expression for the hydrostatic stress (σ_m) can be written as follows:

$$\sigma_m = \frac{1}{3}(\sigma_1 + \sigma_2 + \sigma_3)$$

(or)

$$\sigma_m = \frac{1}{3}(\sigma_r + \sigma_\theta + \sigma_z) \tag{16}$$

Since $\sigma_r = \sigma_\theta$, the Eq. 16 can be written as follows:

$$\sigma_m = \frac{1}{3}[\sigma_z + 2\sigma_\theta] \tag{17}$$

The Eq. 17 can be rearranged as follows for the determination of the stress ratio (σ_m/σ_z):

$$\frac{\sigma_m}{\sigma_z} = \frac{1}{3}\left(1 + \frac{2\sigma_\theta}{\sigma_z}\right) \tag{18}$$

The effective stress can be determined from the following expression as explained elsewhere [19].

$$\sigma_1^2 + \sigma_2^2 + \sigma_3^2 - R^2(\sigma_1\sigma_2 + \sigma_2\sigma_3 + \sigma_3\sigma_1) = (2R^2 - 1)\sigma_{eff}^2$$

This expression can be written as follows in terms of cylindrical coordinates:

$$\sigma_{eff}^2 = \frac{\sigma_z^2 + \sigma_\theta^2 + \sigma_r^2 - R^2(\sigma_z\sigma_\theta + \sigma_\theta\sigma_r + \sigma_r\sigma_z)}{(2R^2 - 1)} \tag{19}$$

Since $\sigma_r = \sigma_\theta$ for cylindrical axisymmetric upsetting or forging operation, the Eq. 19 is as follows:

$$\sigma_{eff}^2 = \frac{\sigma_z^2 + 2\sigma_\theta^2 - R^2(\sigma_z\sigma_\theta + \sigma_\theta^2 + \sigma_\theta\sigma_z)}{(2R^2 - 1)} \tag{20}$$

The Eq. 20 can be rearranged as below for the determination of the stress ratio (σ_{eff}/σ_z).

$$\frac{\sigma_{eff}}{\sigma_z} = \left[\frac{1 + 2\left(\frac{\sigma_\theta}{\sigma_z}\right)^2 - R^2\left(2\left(\frac{\sigma_\theta}{\sigma_z}\right) + \left(\frac{\sigma_\theta}{\sigma_z}\right)^2\right)}{(2R^2 - 1)}\right]^{1/2} \tag{21}$$

The stress formability index (β) provided in the Eq. 11 can be derived for the triaxial stress state condition from the Eqs. 18 and 21 as follows:

$$\beta = 3\{[\sigma_m/\sigma_z]/[1/[\sigma_{eff}/\sigma_z]]\} \tag{22}$$

Different stress ratio parameters, namely, ($\sigma_\theta/\sigma_{eff}$), ($\sigma_m/\sigma_{eff}$) and ($\sigma_z/\sigma_{eff}$) are expressed as follows:

$$(\sigma_\theta/\sigma_{eff}) = \{(\sigma_\theta/\sigma_z)/(\sigma_{eff}/\sigma_z)\} \tag{23}$$

$$(\sigma_m/\sigma_{eff}) = \{(\sigma_m/\sigma_z)/(\sigma_{eff}/\sigma_z)\} \tag{24}$$

$$(\sigma_z/\sigma_{eff}) = [1/(\sigma_{eff}/\sigma_z)] \tag{25}$$

The ratios namely, (σ_θ/σ_z), (σ_m/σ_z) and (σ_{eff}/σ_z) can be determined from the Eqs. 15, 18 and 21, respectively.

Figure 1 shows the flow chart for computing the stress formability index (β), expressed in the Eq. 22.

Experimental details

Iron powder of –150 micron, extra fine Graphite powder and Titanium Carbide powder (–48 micron) were procured and properly mixed to get alloys of Titanium carbide steel composites of the following compositions in a ball mill.

(i) Fe–1.0%C–3%TiC
(ii) Fe–1.0%C–4%TiC

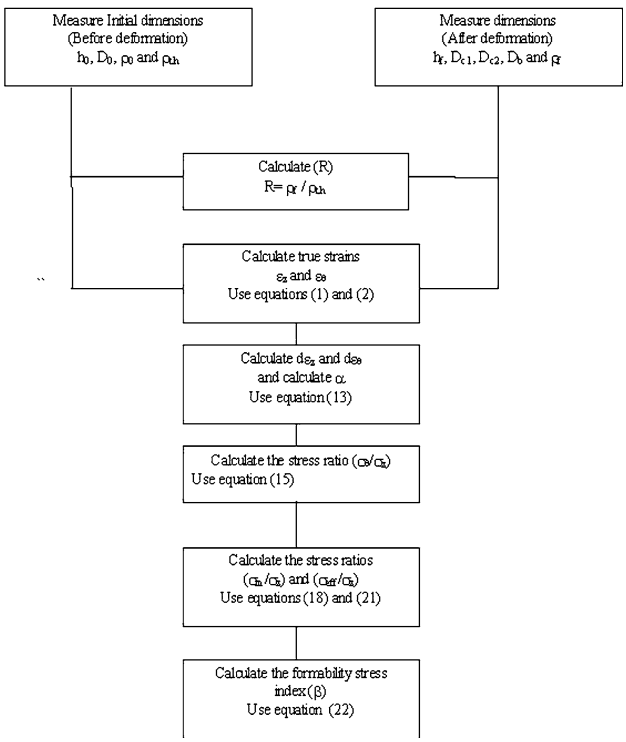

Fig. 1 Flow chart for the determination of workability parameter (β) under triaxial stress state condition

Table 1 Characteristics of iron powder

Sieve size in microns	+125	+106	+90	+63	+53	+37	–37
wt% retained	2.12	26.94	0.00	25.84	21.66	16.77	6.51

(a) Flow rate : 24.5 s /50 gm;

(b) apparent density :3.26 gm/cc;

(c) compressibility : 6.20 gm/cc at a pressure of 4.1 tons/cm^2 (1 tonf/cm^2=98.1 MPa)

Characteristics of Fe–1.0%C–3%TiC powder

(a) Apparent density : 3.436 gm/cc

(b) Compressibility : 6.368 gm/cc at a pressure of 146.67 Mpa.

Characteristics of Fe–1.0%C–4%TiC powder

(c) Apparent density : 3.438 gm/cc

(d) Compressibility : 6.346 gm/cc at a pressure of 146.67 Mpa.

The ball mill was operated for sufficient time to get a homogenized mixture of alloys in the steel. The characterization of the iron powder and the different titanium carbide steel composite powders (3%TiC and 4%TiC) is shown in the Table 1. The compacts were prepared from Fe–1.0%C–3% TiC and Fe–1.0%C–4% TiC powders with different aspect ratios using 100 tonnes capacity Universal Testing Machine. The three different aspect ratios used are shown in the Table 2.

The compacting pressure was controlled so as to obtain density levels of 7.656 ± 0.001 g/cc and 7.612 ± 0.001 g/cc for the steel composites of 3%TiC and 4%TiC content respectively. The compacts were coated on all surfaces with an indigenously developed ceramic coating [22]. This coating was allowed to dry for a period of 6 h at normal atmospheric conditions. Recoating was given to the compacts in the direction 90° to that of the earlier coating. The second coating was allowed to dry in the same condition of the first coating for a further period of 12 h. These coatings were necessary to avoid oxidation of compacts during sintering. Ceramic-coated compacts were sintered in an electric muffle furnace at a temperature of 1120 °C for a period of 60 min.

After the sintering operation, the preforms were upset-forged at a temperature of 1120 °C to the different levels of height strain using a 100 tonnes capacity Friction Screw Press. The forging operation was carried out with no lubricant. The density of forged preforms was determined using the Archimedes principle. After the above-mentioned forging schedule, the dimensions namely, the height of forged specimen (h_f), the contact diameter (D_{c1} and D_{c2}) of top and bottom surfaces, the bulged diameter (D_b) and the barrel radius (R_1) were measured. Initial dimensions of the specimen (Initial height h_o, Initial diameter D_o) and the initial preform density, ρ_o, were measured for each preform before conducting the experiment. The SEM photograph of the iron powder is shown in Fig. 2. The shape dimensions of initial and deformed preforms measured during the experiment are shown in Fig. 3.

Table 2 Initial parameters of the (a) Fe–1.0%C–3%TiC and (b) Fe–1.0%C–4%TiC Sintered P/M preforms

Aspect ratio	Initial Height (h_0) mm	Initial Diameter (D_0) mm	Theoretical preform Density (ρ_{th}) g/cc
(a) Fe–1.0%C–3%TiC			
0.45	11.88	26.36	7.656
0.71	19.05	26.66	7.656
1.25	33.06	26.43	7.656
(b) Fe–1.0%C–4%TiC			
0.45	11.69	25.94	7.612
0.71	18.77	26.27	7.612
1.25	32.68	26.08	7.612

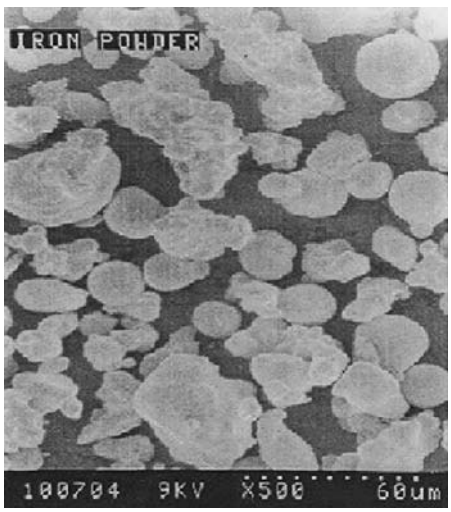

Fig. 2 SEM photograph of iron powder

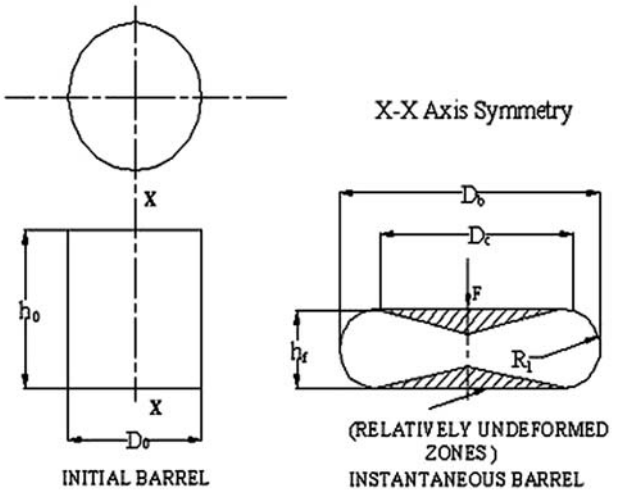

Fig. 3 Upset-forging test preform before and after deformatin

Results and discussion

Figure 4 has been drawn between the formability stress index (β) under triaxial stress state condition and the axial strain (ε_z) for TiC composite steel with varying TiC contents and aspect ratios. This plot shows that the formability stress index (β) value increases with increasing axial strain (ε_z) for any given aspect ratio tested. However, it has been observed that for equal height strain level, the formability stress index value for the smaller aspect ratio is higher compared to that of larger aspect ratio. The above finding of higher stress formability index for smaller aspect ratio preforms is due to the presence of fine pores, and the high magnitude of hydrostatic stress (σ_m) developed to close the pores during hot upsetting. Addition of TiC content in the steel composite leads to formation of coarse pores in the preform which results in lower formability stress index (β) value during the deformation compared to that of the steel composite having lesser amount of TiC content for any given aspect ratio tested. It is found that the formability stress index (β) obtained for 4% TiC is less comparing with 3% TiC composite for any given aspect ratio because of the presence of more pores in the higher addition of TiC. Among the different curve fitting techniques employed, the polynomial curve of second order was found to be fit for relating the axial strain (ε_z) and the formability stress index (β). Empirical constants established for the polynomial equation which relates the above two parameters are as shown in the Table 3. From the Table 3, it has been observed that the constant term for ε_z^2 decreases, while that of ε_z increases, with increasing level of aspect ratio.

Figure 5a–c shows the plot drawn between the relative density (R) and the axial strain (ε_z) for steel composites with varying TiC contents and aspect ratios. It is observed that for any given aspect ratio tested, the increase in addition of TiC content decreases the relative density. However, the fracture strain is increased as the TiC content in the steel composite increases. Higher relative density (R) value is observed in the lower aspect ratio preforms in which the rate of pore closure is faster due to small pores bed height. As shown in the Fig. 5a, three different densification mechanisms with different slope

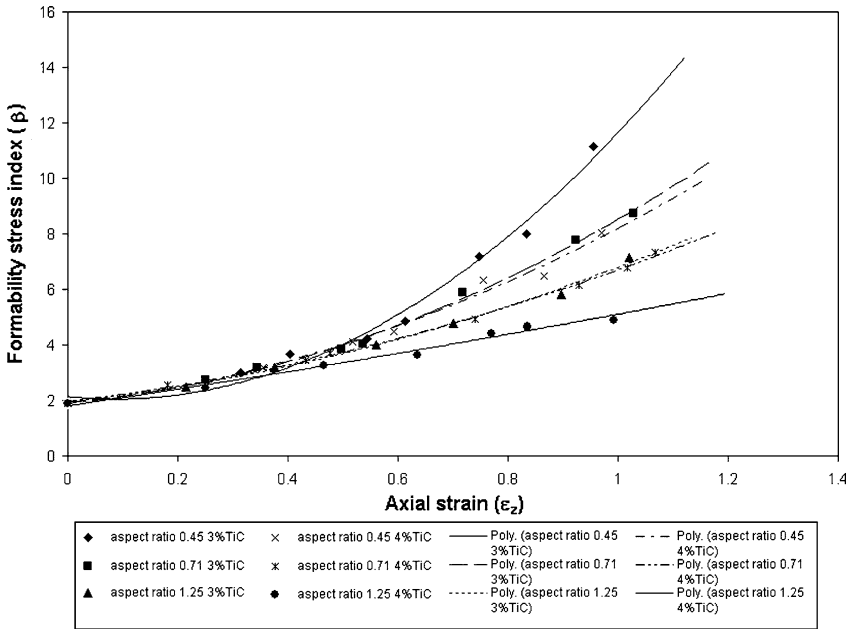

Fig. 4 Variation of formability stress index (β) with respect to the axial strain (ε_z) for triaxial condition

Table 3 Curve fitting results—axial strain (ε_z) versus Formability stress index (β)

Aspect ratio	Fractional preform density	Name of the curve	
		Polynomial equation	R_2^2
Formability stress index (β) versus Axial strain(ε_z) Fe–1.0%C–3%TiC			
0.45	0.8318	$\beta = 11.453\varepsilon_z^2$–1.9394x + 2.131	0.9842
0.71	0.8317	$\beta = 4.9125\varepsilon_z^2 + 1.6737x + 1.9364$	0.9964
1.25	0.8317	$\beta = 2.7306\varepsilon_z^2 + 2.1242x + 1.9473$	0.9947
Formability stress index (β) versus Axial strain(ε_z) Fe–1.0%C–4%TiC			
0.45	0.8288	$\beta = 4.98\varepsilon_z^2 + 2.2199x + 1.886$	0.9872
0.71	0.8288	$\beta = 2.4043\varepsilon_z^2 + 2.3325x + 1.9675$	0.9981
1.25	0.8288	$\beta = 0.3906\varepsilon_z^2 + 2.9057x + 1.8118$	0.9821

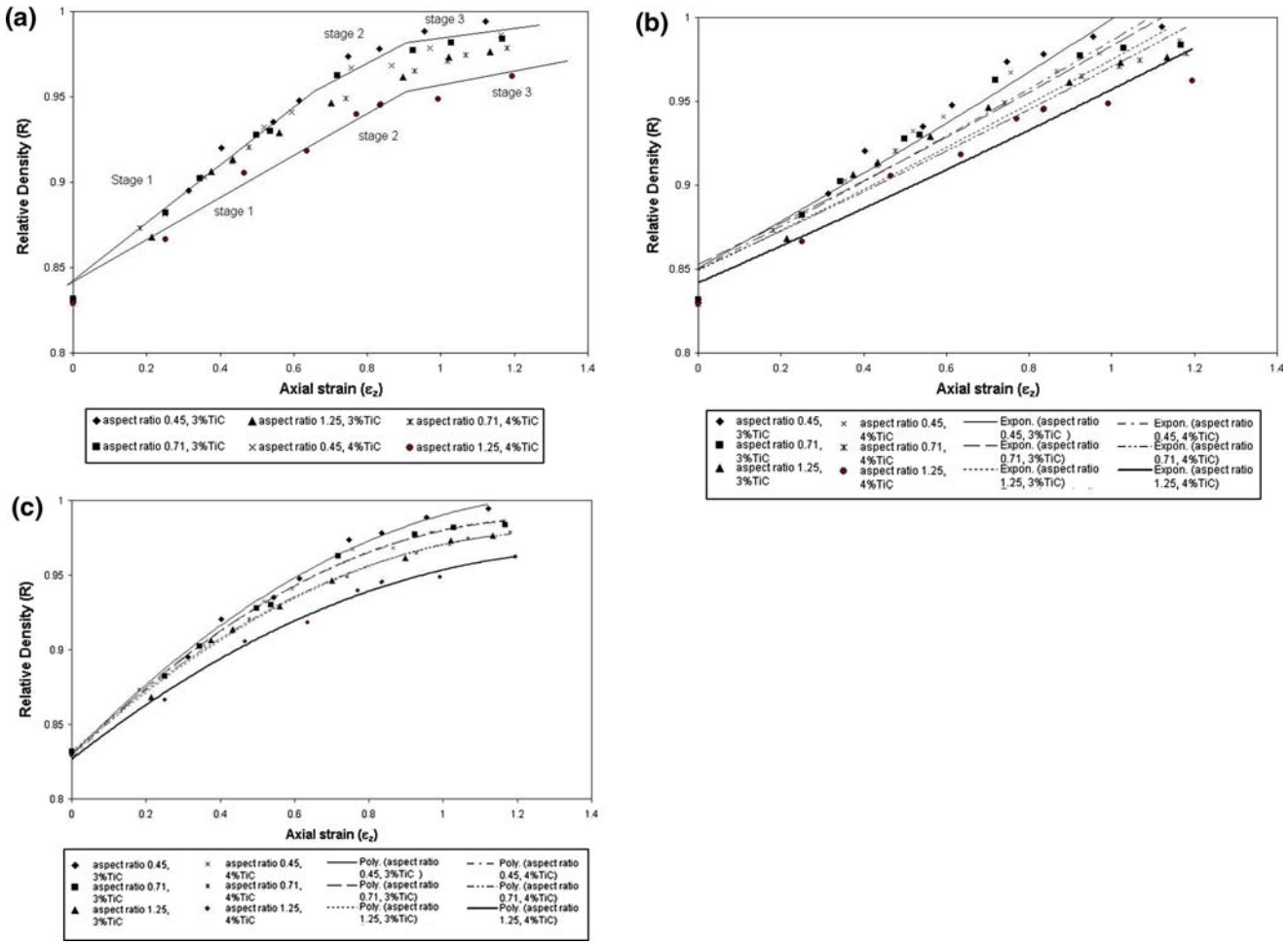

Fig. 5 The variation of relative density (R): (**a**) with respect to the axial strain (ε_z); (**b**) with respect to the axial strain (ε_z) (exponential curve fitting); (**c**) with respect to the axial strain (ε_z) (polynomial curve fitting)

values are operative during the deformation. Stage I represents initial deformation with rapid densification due to the initial pore closure followed by Stage II and Stage III which represent the formation of bulging, and the subsequent appearance of crack and the occurrence of fracture, respectively. Table 4 shows the slope of various stages of densification for lower and higher aspect ratios tested. Two different curve fitting techniques, namely, exponential and polynomial are employed to establish the relation between the axial strain (ε_z) and the relative

Table 4 Slope of various densification mechanisms obtained between the relative density (R) and the axial strain (ε_z)

Relationship	TiC content	Aspect ratio	Slope
R versus ε_z	3% and 4%	0.45	0.9, 0.7 and 0.176
		0.71	
	3% and 4%	1.25	0.83, 0.53 and 0.23

density (R). Polynomial curve fitting, as shown in Fig. 5c, with correlation coefficient (R_2^2) value close to 1.0, found to be fit. The relationship established in different curve fittings and their corresponding correlation coefficient values (R_2^2) are provided in Table 5.

Figure 6 has been drawn between the Poisson's ratio (γ) and the relative density (R) for TiC composite steels with varying TiC contents and aspect ratios. It is observed that the Poisson's ratio increases with increasing value of relative density (R). A larger Poisson's ratio value is observed for higher aspect ratio preforms which exhibit more bulging compared to that of the smaller aspect ratio preforms. A straight line relationship is established between the relative density (R) and the Poisson's ratio (γ). Slope of the straightline relationship obtained for different aspect ratio tested are provided in Table 6.

Figure 7a–d have been developed between the relative density (R) and the stress ratio parameter ($\sigma_\theta/\sigma_{\text{eff}}$) under triaxial stress state condition for steel composites with

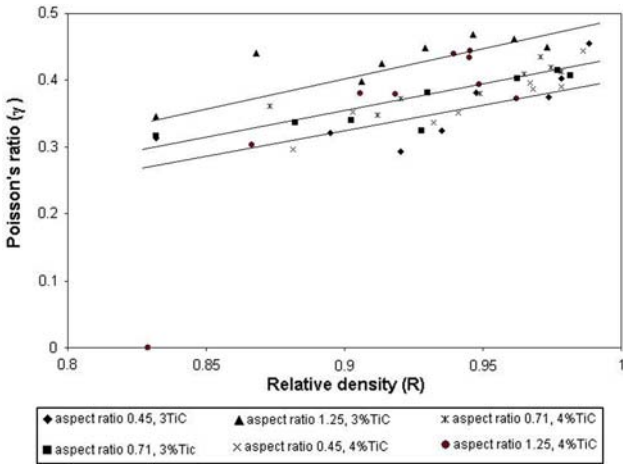

Fig. 6 The variation of the Poisson's ratio (g) with respect to the relative density (R)

varying TiC contents and aspect ratios. As the relative density (R) increases, the stress ratio parameter ($\sigma_\theta/\sigma_{\text{eff}}$) value also increases during hot upsetting. The hoop stress, σ_θ, keeps on increasing as densification progresses during the deformation. As shown in Fig. 7a, there are three different densification mechanisms operative for the larger aspect ratio preforms compared to four such different mechanisms operative in the case of smaller and medium aspect ratios. Stage I of the densification

Table 5 Curve fitting results—relative density (R) versus axial strain (ε_z)

Aspect ratio	Fractional preform density	Name of the curve	
		Exponential equation	R_2^2
Relative density (R) versus axial strain (ε_z) Fe–1.0%C–3%TiC			
0.45		$R = 0.8508e^{0.1608\varepsilon_z}$	0.936
0.71		$R = 0.8528e^{0.1421\varepsilon_z}$	0.9258
1.25		$R = 0.8493e^{0.138\varepsilon_z}$	0.9381
Relative density (R) versus axial strain (ε_z) Fe–1.0%C–4%TiC			
0.45	0.8288	$R = 0.8501e^{0.1487\varepsilon_z}$	0.9241
0.71	0.8288	$R = 0.8498e^{0.133\varepsilon_z}$	0.9424
1.25	0.8288	$R = 0.8419e^{0.1283\varepsilon_z}$	0.9393
		Polynomial equation	R_2^2
Relative density (R) versus axial strain (ε_z) Fe–1.0%C–3%TiC			
0.45		$R = -0.0918\ \varepsilon_z^2 + 0.2524\varepsilon_z + 0.8298$	0.9942
0.71		$R = -0.0961\varepsilon_z^2 + 0.2467\varepsilon_z + 0.8293$	0.9966
1.25		$R = -0.0846\varepsilon_z^2 + 0.2252\varepsilon_z + 0.8299$	0.9963
Relative density (R) versus Axial strain (ε_z) Fe–1.0%C–4%TiC			
0.45	0.8288	$R = -0.0991\varepsilon_z^2 + 0.2521\varepsilon_z + 0.8273$	0.9974
0.71	0.8288	$R = -0.0855\varepsilon_z^2 + 0.2245\varepsilon_z + 0.8315$	0.9986
1.25	0.8288	$R = -0.069\varepsilon_z^2 + 0.1959\varepsilon_z + 0.8266$	0.9929

Table 6 Curve fitting results—relative density (R) versus Poisson's ratio (γ)

Relationship	TiC content	Aspect ratio	Slope
R versus γ	3% and 4%	0.45	0.267
	3% and 4%	0.71	0.194
	3% and 4%	1.25	0.176

Table 7 Slope of various densification mechanisms obtained between the stress ratio ($\sigma_\theta/\sigma_{\text{eff}}$) and the relative density (R)

Relationship	TiC content	Aspect ratio	Slope
($\sigma_\theta/\sigma_{\text{eff}}$) versus R	3% and 4%	0.45	0.267, 0.554, 1.106 and 2.355
	3% and 4%	0.71	0.267, 0.554 and 1.106
	3% and 4%	1.25	0.267 and 0.554

mechanism, as shown in Fig. 7a, takes place with a gradual increase of the stress ratio parameter ($\sigma_\theta/\sigma_{\text{eff}}$) values from 0.5 to 1.0 for an increase in the relative density (R) values from 0.83 to 0.91. A moderate increase in both the parameters is observed in Stage II, with relative density reaching a value of 0.94 for a stress ratio ($\sigma_\theta/\sigma_{\text{eff}}$) value of 1.75 followed by Stage III with steep increase in stress ratio value close to 3.0 with relative density value reaches 0.97. Stage IV represents the final phase of the deformation with relative density touches 0.98 and the stress ratio parameter ($\sigma_\theta/\sigma_{\text{eff}}$) attained a value of 3.8. Table 7 shows the slope of the different straight line represents various stages of densification of the preforms during the deformation. Figure 7b–d show different curve fitting techniques employed between the above two parameters, namely, the stress ratio ($\sigma_\theta/\sigma_{\text{eff}}$) and the relative density (R). The respective equation determined for each curve fitting technique for each aspect ratio tested and their corresponding correlation coefficient (R_2^2) are shown in

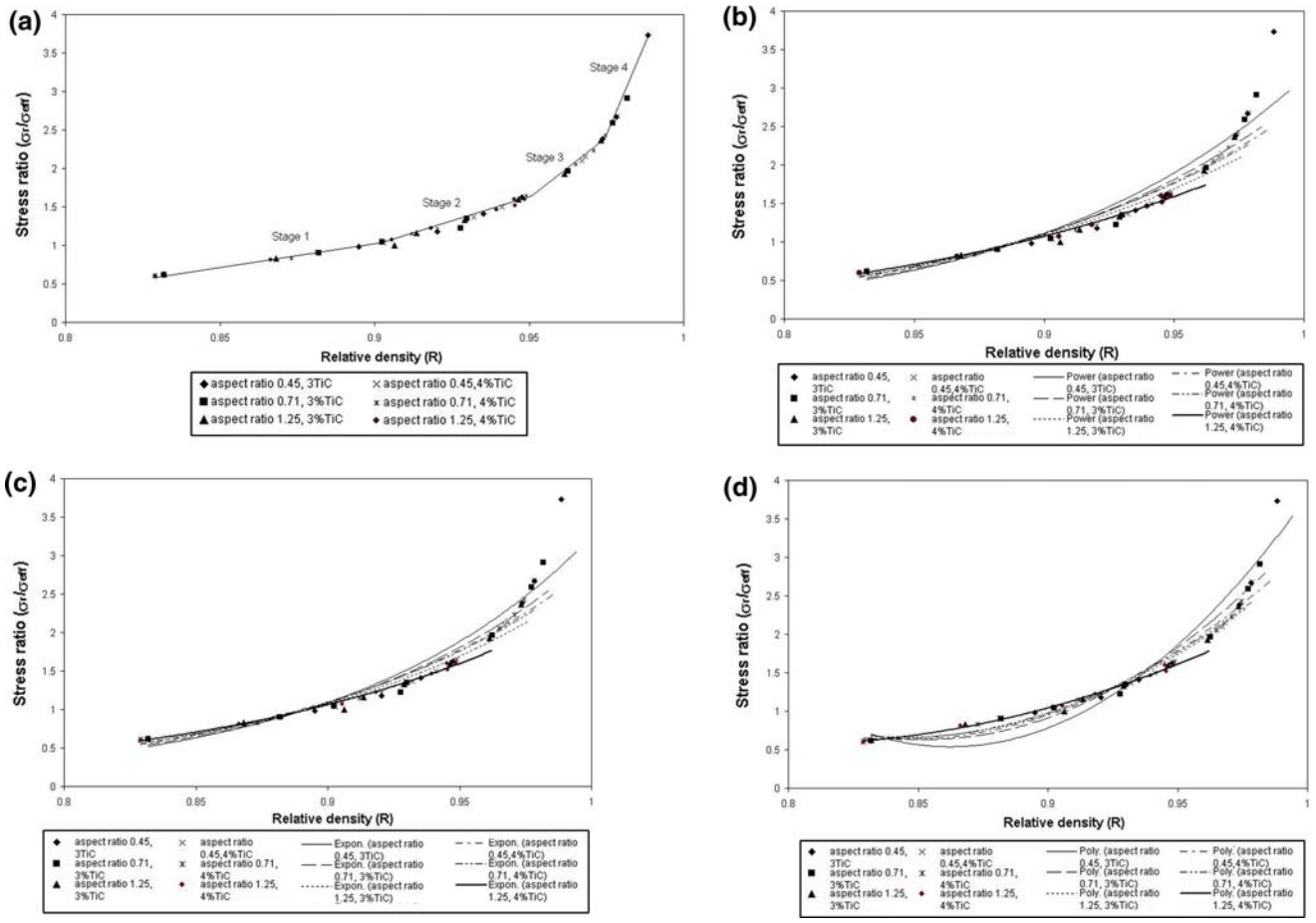

Fig. 7 The variation of the stress ratio ($\sigma_\theta/\sigma_{\text{eff}}$): (**a**) with respect to the relative density (R); (**b**) with respect to the relative density (R) (power law curve fitting); (**c**) with respect to the relative density(R) (Exponential curve fitting); (**d**) with respect to the relative density(R) (polynomial curve fitting)

Table 8 Curve fitting results—stress ratio ($\sigma_\theta/\sigma_{eff}$) versus relative density (R)

Aspect ratio	Fractional preform density	Name of the curve	
		Power law equation	R_2^2
Stress ratio ($\sigma_\theta/\sigma_{eff}$) versus relative density (R) Fe–1.0%C–3%TiC			
0.45	0.8318	$\sigma_\theta/\sigma_{eff} = 3.1439\ R^{9.8452}$	0.9221
0.71	0.8317	$\sigma_\theta/\sigma_{eff} = 2.9076\ R^{9.2143}$	0.945
1.25	0.8318	$\sigma_\theta/\sigma_{eff} = 2.5727\ R^{8.1692}$	0.9587
Stress ratio ($\sigma_\theta/\sigma_{eff}$) versus relative density (R) Fe–1.0%C–4%TiC			
0.45	0.8288	$\sigma_\theta/\sigma_{eff} = 2.7798\ R^{8.7256}$	0.9656
0.71	0.8288	$\sigma_\theta/\sigma_{eff} = 2.7223\ R^{8.4683}$	0.9735
1.25	0.8288	$\sigma_\theta/\sigma_{eff} = 2.3082\ R^{7.2666}$	0.9947
		Exponential equation	R_2^2
Stress ratio ($\sigma_\theta/\sigma_{eff}$) versus relative density (R) Fe–1.0%C–3%TiC			
0.45	0.8318	$\sigma_\theta/\sigma_{eff} = 6E\text{–}05e^{10.892\ R}$	0.9349
0.71	0.8317	$\sigma_\theta/\sigma_{eff} = 0.0001e^{10.193\ R}$	0.9554
1.25	0.8318	$\sigma_\theta/\sigma_{eff} = 0.0003e^{9.0971\ R}$	0.9666
Stress ratio ($\sigma_\theta/\sigma_{eff}$) versus relative density (R) Fe–1.0%C–4%TiC			
0.45	0.8288	$\sigma_\theta/\sigma_{eff} = 0.0002e^{9.6817\ R}$	0.9732
0.71	0.8288	$\sigma_\theta/\sigma_{eff} = 0.0002e^{9.3999\ R}$	0.9802
1.25	0.8288	$\sigma_\theta/\sigma_{eff} = 0.0007e^{8.1621\ R}$	0.9962
		Polynomial equation	R_2^2
Stress ratio ($\sigma_\theta/\sigma_{eff}$) versus relative density (R) Fe–1.0%C–3%TiC			
0.45	0.8318	$\sigma_\theta/\sigma_{eff} = 172.29\ R^2 - 297.16\ R + 128.67$	0.942
0.71	0.8317	$\sigma_\theta/\sigma_{eff} = 126.4\ R^2 - 215.58\ R + 92.552$	0.9742
1.25	0.8318	$\sigma_\theta/\sigma_{eff} = 96.055\ R^2 - 162.17\ R + 69.11$	0.9837
Stress ratio ($\sigma_\theta/\sigma_{eff}$) versus relative density (R) Fe–1.0%C–4%TiC			
0.45	0.8288	$\sigma_\theta/\sigma_{eff} = 102.93\ R^2 - 173.74\ R + 73.953$	0.9759
0.71	0.8288	$\sigma_\theta/\sigma_{eff} = 91.973\ R^2 - 154.39\ R + 65.432$	0.9888
1.25	0.8288	$\sigma_\theta/\sigma_{eff} = 43.58\ R^2 - 69.267\ R + 28.085$	0.9945

Table 8. Polynomial curve fitting with good correlation coefficient value (very close to 1.0) is found to be fit for relating the above two parameters. It has been observed that, from the equation obtained for the selected polynomial curve fitting that the constant term of the R^2 term and the independent constant are decreasing with the increasing level of aspect ratio.

Figure 8a–d have been developed between the relative density (R) and the stress ratio parameter (σ_m/σ_{eff}) under triaxial stress state condition for steel composites with varying TiC contents and aspect ratios. As the relative density (R) increases the stress ratio parameter (σ_m/σ_{eff}) also increases during hot upsetting. The hydrostatic stress, σ_m, keeps on increasing as densification progresses during the deformation. As shown in Fig. 7a, there are three different densification mechanisms operative for the larger aspect ratio preforms compared to four different such mechanisms operative in the case of smaller and medium aspect ratios. Stage I of the densification mechanism, as shown in Fig. 8a, takes place with a gradual increase of the stress ratio parameter (σ_m/σ_{eff}) values from 0.5 to 1.0 for an increase in the relative density (R) values from 0.83 to 0.91. A moderate increase in both the parameters is observed in Stage II, with relative density reaching a value of 0.94 for a stress ratio (σ_m/σ_{eff}) value of 1.5 followed by Stage III with steep increase in stress ratio value close to 2.5 with relative density value of 0.97. Stage IV represents the final phase of the deformation with relative density touching 0.98 and the stress ratio (σ_m/σ_{eff}) attained a value of 3.75. Table 9 shows the slope of the different straight lines represents various stages of densification of the preforms during the deformation. Figure 8b–d show different curve fitting techniques employed between the

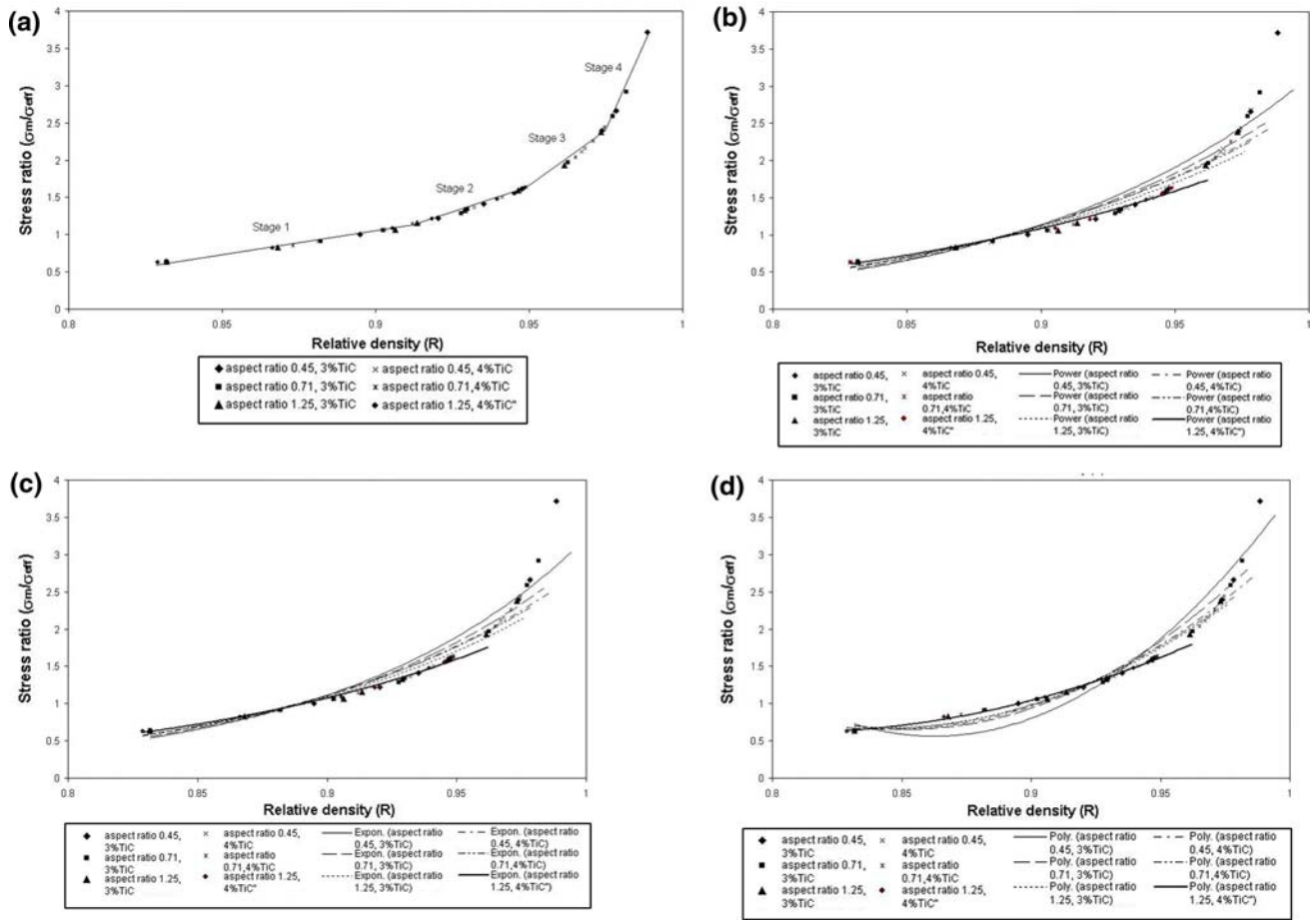

Fig. 8 The variation of the stress ratio (σ_m/σ_{eff}): (**a**) with respect to the relative density (R); (**b**) with respect to the relative density (R) (Power law curve fitting); (**c**) with respect to the relative density (R) (Exponential curve fitting); (**d**) with respect to the relative density (R) (Polynomial curve fitting)

Table 9 Slope of various densification mechanisms obtained between the stress ratio (σ_m/σ_{eff}) and the relative density (R)

Relationship	TiC content	Aspect ratio	Slope
(σ_m/σ_{eff}) versus R	3% and 4%	0.45	0.176, 0.424, 0.839 and 2.355
	3% and 4%	0.71	0.176, 0.424 and 0.839
	3% and 4%	1.25	0.176 and 0.424

above two parameters, namely, the stress ratio (σ_m/σ_{eff}) and the relative density (R). The respective equation determined for each curve fitting technique for each aspect ratio tested and the corresponding correlation coefficient (R_2^2) are shown in Table 10. Polynomial curve fitting with good correlation coefficient value (very close to 1.0) is found to be fit for relating the above two parameters. It has been observed, from the equation obtained for the selected polynomial curve fitting that the constant term of the R^2 term and the independent constant are decreasing with the increasing level of the aspect ratio.

Figure 9a–d have been developed between the relative density (R) and the stress ratio parameter (σ_z/σ_{eff}) under triaxial stress state condition for steel composites with varying TiC contents and aspect ratios. As the relative density (R) increases the stress ratio parameter (σ_z/σ_{eff}) also increases during hot upsetting. The axial stress, σ_z, keeps on increasing as relatively larger amount of load is required to continue the deformation. As shown in Fig. 7a, there are three different densification mechanisms operative for the larger aspect ratio preforms compared to four such different mechanisms operative in the case of smaller and medium aspect ratios. Stage I of the densification mechanism, as shown in Fig. 9a, takes place with a gradual increase of the stress ratio parameter (σ_z/σ_{eff}) values from 0.6 to 1.0 for an increase in the relative density (R) values from 0.83 to 0.92. A moderate increase

Table 10 Curve fitting results—stress ratio (σ_m/σ_{eff}) versus relative density (R)

Aspect ratio	Fractional preform density	Name of the curve	
		Power law equation	R_2^2
Stress ratio (σ_m/σ_{eff}) versus relative density (R) Fe–1.0%C–3%TiC			
0.45	0.8318	$\sigma_m/\sigma_{eff} = 3.122\ R^{9.5961}$	0.9174
0.71	0.8317	$\sigma_m/\sigma_{eff} = 2.5697\ R^{8.0294}$	0.9459
1.25	0.8318	$\sigma_m/\sigma_{eff} = 2.5697\ R^{8.0294}$	0.9631
Stress ratio (σ_m/σ_{eff}) versus relative density (R) Fe–1.0%C–4%TiC			
0.45	0.8288	$\sigma_m/\sigma_{eff} = 2.7554\ R^{8.4942}$	0.9612
0.71	0.8288	$\sigma_m/\sigma_{eff} = 2.7095\ R^{8.3131}$	0.9692
1.25	0.8288	$\sigma_m/\sigma_{eff} = 2.2806\ R^{7.0493}$	0.9934
		Exponential equation	R_2^2
Stress ratio (σ_m/σ_{eff}) versus relative density (R) Fe–1.0%C–3%TiC			
0.45	0.8318	$\sigma_m/\sigma_{eff} = 8E\text{-}05e^{10.619\ R}$	0.9306
0.71	0.8317	$\sigma_m/\sigma_{eff} = 0.0001e^{9.969\ R}$	0.9565
1.25	0.8318	$\sigma_m/\sigma_{eff} = 0.0003e^{8.9415\ R}$	0.9711
Stress ratio (σ_m/σ_{eff}) versus relative density (R) Fe–1.0%C–4%TiC			
0.45	0.8288	$\sigma_m/\sigma_{eff} = 0.0002e^{9.4285\ R}$	0.9696
0.71	0.8288	$\sigma_m/\sigma_{eff} = 0.0003e^{9.2301\ R}$	0.9764
1.25	0.8288	$\sigma_m/\sigma_{eff} = 0.0009e^{7.9218\ R}$	0.9959
		Polynomial equation	R_2^2
Stress ratio (σ_m/σ_{eff}) versus relative density (R) Fe–1.0%C–3%TiC			
0.45	0.8318	$\sigma_m/\sigma_{eff} = 171.07\ R^2 - 295.14\ R + 127.86$	0.9405
0.71	0.8317	$\sigma_m/\sigma_{eff} = 124.44\ R^2 - 212.14\ R + 91.066$	0.975
1.25	0.8318	$\sigma_m/\sigma_{eff} = 95.031\ R^2 - 160.39\ R + 68.353$	0.9846
Stress ratio (σ_m/σ_{eff}) versus relative density (R) Fe–1.0%C–4%TiC			
0.45	0.8288	$\sigma_m/\sigma_{eff} = 103.51\ R^2 - 174.97\ R + 74.589$	0.9771
0.71	0.8288	$\sigma_m/\sigma_{eff} = 94.076\ R^2 - 158.27\ R + 67.223$	0.987
1.25	0.8288	$\sigma_m/\sigma_{eff} = 48.422\ R^2 - 78.021\ R + 32.04$	0.9979

in both the parameters is observed in Stage II, with relative density reaching a value of 0.95 for a stress ratio (σ_z/σ_{eff}) value of 1.75 followed by Stage III with steep increase in stress ratio value close to 3.0 with relative density value of 0.975. Stage IV represents the final phase of the deformation with relative density touching 0.98 and the stress ratio (σ_z/σ_{eff}) attained a value of 3.8. Table 11 shows the slope of the different straight lines represents various stages of densification of the preforms during the deformation. Figure 9b–d show different curve fitting techniques employed between the above two parameters, namely, the stress ratio (σ_z/σ_{eff}), and the relative density (R). The respective equation determined for each curve fitting technique for each aspect ratio tested and their corresponding correlation coefficient (R_2^2) are shown in Table 12. Polynomial curve fitting with good correlation coefficient value (very close to 1.0) is found to be fit for relating the above two parameters. It has been observed from the equation obtained for the selected polynomial curve fitting, the constant term of the R^2 term and the independent constant are decreasing with the increasing level of aspect ratio.

Figure 10 has been plotted between the formability stress index parameter (β) and the fracture strain for steel composites with varying percentage content of TiC and aspect ratios. It is observed that the fracture strain is found almost constant for different TiC contents and aspect ratios. However, the formability stress index parameter (β) varies with the percent content of TiC and aspect ratios tested. This parameter has been found to be high for lower aspect ratio and lower TiC content in the composite.

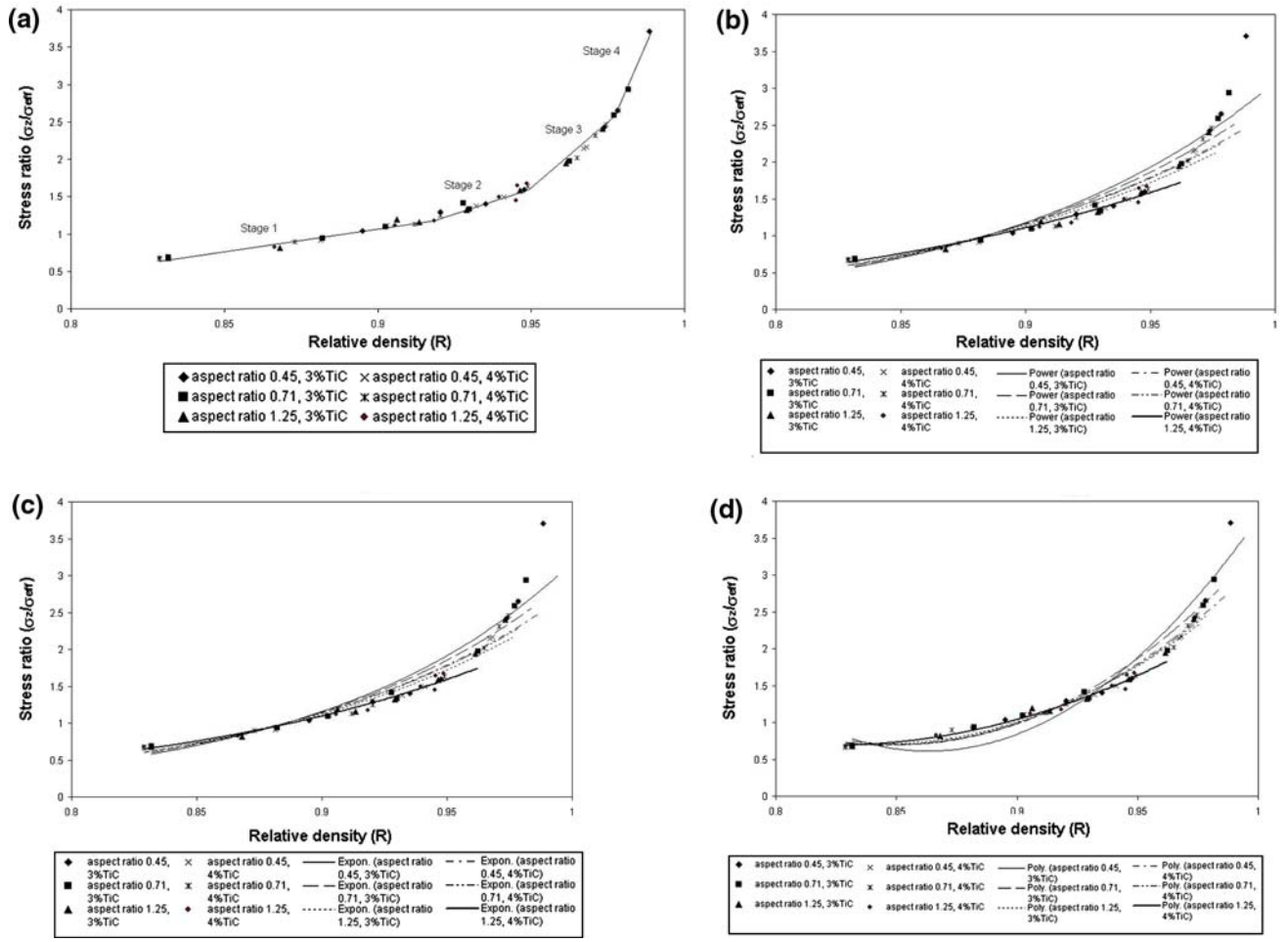

Fig. 9 The variation of the stress ratio (σ_z/σ_{eff}): (**a**) with respect to the relative density (R); (**b**) with respect to the relative density (R) (Power law curve fitting); (**c**) with respect to the relative density (R) (Exponential curve fitting); (**d**) with respect to the relative density (R) (Polynomial curve fitting)

Table 11 Slope of various densification mechanisms obtained between the stress ratio (σ_z/σ_{eff}) and the relative density (R)

Relationship	TiC content	Aspect ratio	Slope
(σ_z/σ_{eff}) versus R	3% and 4%	0.45	0.176, 0.466, 1.191 and 2.747
	3% and 4%	0.71	0.176, 0.466 and 1.191
	3% and 4%	1.25	0.176 and 0.466

Conclusion

The following conclusions can be drawn from the present analysis of the work:

- For any given aspect ratio tested, the increase in addition of TiC content decreases the densification and thereby the formability behaviour of the preform.
- Different densification mechanisms operative during hot upsetting of preforms were investigated. Four different mechanisms are operative for the lower aspect ratio preforms, the slope of the mechanisms obtained were determined. Influence of TiC addition, in the steel composite, on the densification mechanism was studied. Addition of titanium carbide in the composite steel reduces the maximum stress ratio attained during the deformation.
- A relationship between the stress ratios namely, ($\sigma_\theta/\sigma_{eff}$), ($\sigma_m/\sigma_{eff}$) and ($\sigma_z/\sigma_{eff}$), under triaxial stress state condition and relative density (R) was established for varying content of TiC in the composite and aspect ratios.
- The stress formability index (β) as expressed theoretically as a function of axial strain (ε_z), and empirical constants for the expressions were found experimentally.

Table 12 Curve fitting results—stress ratio (σ_z/σ_{eff}) versus relative density (R)

Aspect ratio	Fractional preform density	Name of the curve	
		Power law equation	R_2^2
Stress ratio (σ_z/σ_{eff}) versus relative density (R) Fe–1.0%C–3%TiC			
0.45	0.8318	$\sigma_z/\sigma_{eff} = 3.0806\ R^{9.1226}$	0.9058
0.71	0.8317	$\sigma_z/\sigma_{eff} = 2.8959\ R^{8.6248}$	0.9428
1.25	0.8318	$\sigma_z/\sigma_{eff} = 2.5634\ R^{7.7683}$	0.956
Stress ratio (σ_z/σ_{eff}) versus relative density (R) Fe–1.0%C–4%TiC			
0.45	0.8288	$\sigma_z/\sigma_{eff} = 2.7105\ R^{8.059}$	0.9498
0.71	0.8288	$\sigma_z/\sigma_{eff} = 2.6851\ R^{8.0151}$	0.9579
1.25	0.8288	$\sigma_z/\sigma_{eff} = 2.2259\ R^{6.6291}$	0.9688
		Exponential equation	R_2^2
Stress ratio (σ_z/σ_{eff}) versus relative density (R) Fe–1.0%C–3%TiC			
0.45	0.8318	$\sigma_z/\sigma_{eff} = 0.0001e^{10.099\ R}$	0.9196
0.71	0.8317	$\sigma_z/\sigma_{eff} = 0.0002e^{9.5427\ R}$	0.9536
1.25	0.8318	$\sigma_z/\sigma_{eff} = 0.0005e^{8.6513\ R}$	0.9641
Stress ratio (σ_z/σ_{eff}) versus relative density (R) Fe–1.0%C–4%TiC			
0.45	0.8288	$\sigma_z/\sigma_{eff} = 0.0004e^{8.9522\ R}$	0.9595
0.71	0.8288	$\sigma_z/\sigma_{eff} = 0.0004e^{8.9043\ R}$	0.9661
1.25	0.8288	$\sigma_z/\sigma_{eff} = 0.0013e^{7.4568\ R}$	0.9731
		Polynomial equation	R_2^2
Stress ratio (σ_z/σ_{eff}) versus relative density (R) Fe–1.0%C–3%TiC			
0.45	0.8318	$\sigma_z/\sigma_{eff} = 168.62\ R^2 - 291.09\ R + 126.24$	0.9362
0.71	0.8317	$\sigma_z/\sigma_{eff} = 120.51\ R^2 - 205.25\ R + 88.093$	0.9731
1.25	0.8318	$\sigma_z/\sigma_{eff} = 92.983\ R^2 - 156.83\ R + 66.837$	0.9764
Stress ratio (σ_z/σ_{eff}) versus relative density (R) Fe–1.0%C–4%TiC			
0.45	0.8288	$\sigma_z/\sigma_{eff} = 104.69\ R^2 - 177.42\ R + 75.861$	0.9782
0.71	0.8288	$\sigma_z/\sigma_{eff} = 98.283\ R^2 - 166.02\ R + 70.806$	0.9814
1.25	0.8288	$\sigma_z/\sigma_{eff} = 58.106\ R^2 - 95.528\ R + 39.95$	0.9722

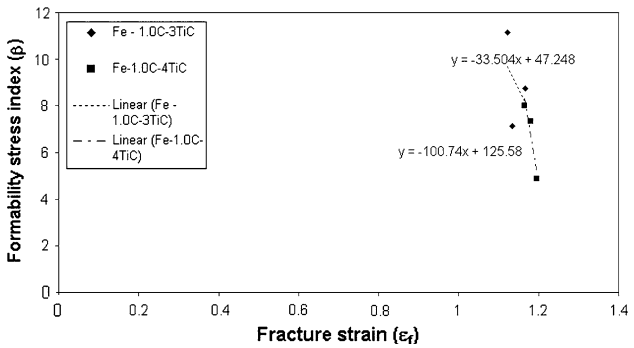

Fig. 10 Variation of the formability stress index (β) under triaxial stress condition with respect to the fracture strain(ε_f)

References

1. Kuhn HA, Lee PW, Erturk T (1973) J Eng Mater-T ASME 95:213–218
2. Lee PW, Kuhn HA (1973) Met Trans 4:969–974
3. Kuhn HA, Downey CL (1971) Int J Powder Metall 7:15–25
4. Shima S, Oyane M (1976) Int J Mech Sci 18:285–291
5. Doraivelu SM, Gegel HL, Gunasekaran JS, Malas JC, Morugan JT (1984) Int J Mech Sci 26(9/10):527–535
6. Abdel-Rahman M, El-Sheikh MN (1995) J Mater Process Technol 54:97–102
7. Sowerby R, O'Reilly I, Chandrasekaran N, Dung NL (1984) J Eng Mater-T ASME 106:101–106
8. Rao KP, Hawbolt EB (1992) J Eng Mater-T ASME 114:116–123
9. Park JJ (1995) Int J Mech Sci 37:709–719

10. Narayanasamy R, Ponalagusamy R (2000) J Mater Process Technol 97:107–109
11. Tvergard V (1982) Int J Fract 18/4:237–252
12. Zhou ZY, Chen PQ, Shao WB, Xia W (2002) J Mater Process Technol 129:385–388
13. Gouveia BPPA, Rodrigues JMC, Martins PAF (2000) J Mater Process Tech 101:52–63
14. Narayansamy R, Ponalagusamy R, Subramanian KR (2001) J Mater Process Technol 110:182–185
15. Venugopal Rao A, Ramkrishnan N, Krishnakumar R (2003) J Mater Process Technol 142:29
16. Feng JP, Luo JZ (2000) . J Mater Process Technol 108:40
17. Narayanasamy R, Pandey KS (1997) J Mater Proc Technol 72:201–207
18. Narayanasamy R, Pandey KS (1997) J Mater Proc Technol 70:17–21
19. Narayansamy R, Pandey KS (2000) J Mater Process Technol 100:84–94
20. Vujovic AH, Shabalk J (1986) J Eng Mater Technol 108:245
21. Narayanasamy R, Ramesh T, Pandey KS (2006) Mater Design 27(7):566–575
22. Narayan R (2001) Ceramic Coatings, IIT, Kanpur, India, Private Communication